X-ray spectrometer simulation code with a detailed support of mosaic crystals

Smid, M.; Pan, X.; Falk, K.;

Originally published:

December 2020

Computer Physics Communications 262(2020), 107881

DOI: https://doi.org/10.1016/j.cpc.2020.107811

Perma-Link to Publication Repository of HZDR:

https://www.hzdr.de/publications/Publ-29826

X-ray spectrometer simulation code with a detailed support of mosaic crystals

Michal Šmíd[a,*], Xiayun Pan[a], Kateřina Falk[a,b,c]

[a] *Helmholtz-Zentrum Dresden-Rossendorf, Dresden, Germany*
[b] *Technische Universität Dresden, Dresden, Germany*
[c] *Institute of Physics ASCR, Prague, Czech Republic*

Abstract

We present a newly developed ray tracing code called *mmpxrt*, dedicated to study and design x-ray crystal optics, with a special focus on mosaic crystal spectrometers. Its main advantage over other currently available ray tracing codes is that it includes detailed and benchmarked algorithm to treat mosaic crystals, especially HOPG and HAPG (Highly Oriented / Annealed Pyrolitic Graphite). The code is dedicated primarily to study crystal spectrometers, therefore their implementation is very straightforward, and the code has mostly automatic evaluation of their performance. It can, however, be used universally to study other crystal instruments, like monochromators, mirrors, and analyzers. The code is publicly available, written in Python3 and is distributed as a Python library with test cases included.

Keywords: mosaic crystal, x-ray spectroscopy, ray tracing, Python3

PROGRAM SUMMARY

Program Title: mmpxrt
Program Repository:
https://gitlab.hzdr.de/smid55/mmpxrt
Licensing provisions: MIT
Programming language: Python 3

1. Introduction

Mosaic crystals have been used for x-ray spectrometers for decades [1, 2], in recent years, they found many applications in high-intensity laser-plasma studies where there a limited amount of photons is detected in each shot and single shot spectra are desirable. Then a high crystal reflectivity is required to obtain measurable signal. This concerns especially applications for x-ray Thomson scattering (XRTS) [3] or laser-driven betatron radiation [4].

First ray tracing model calculating with mosaic crystal was written already in 1991 [5] as a part of the SHADOW code [6]. However, this and later similar codes are not flexible for detailed studies of x-ray spectrometers [7]. Novel code was presented in 2012 [7], however this code is not available for general public. This situation led us to develop a novel code within modern language Python3, optimized to easily model various x-ray spectrometers and similar devices and simple enough to allow users with basic knowledge of the language to run their own cases, allowing the code to be publicly available.

Apart from focus on mosaic crystals, the strength of the code is that it comes with built-in evaluation tool to asses most basic spectrometer parameters and which produces useful graphical output. Its open structure in Python3 language also allows e.g. batch simulations or parameter scans.

*Corresponding author.
E-mail address: m.smid@hzdr.de

2. Code workflow

The code is designed to be powerful and easy-to-use characterization of x-ray spectrometers. The random nature of mosaic crystals implies that a Monte Carlo simulational approach is very suitable. It uses the random nature of a Monte Carlo simulation in two places. First, the properties of each ray are randomly calculated based on given probability distribution of direction, source position, and energy. Second, the interaction with mosaic crystal is governed by random spread of the crystallites and penetration of the x-ray into the crystal.

The code is technically a Python3 library, each simulation is a Python script which loads the library, sets the predefined parameters and runs the simulation. The detailed results, including trajectories of all rays, are stored in python variables as well as saved into an output file and an overview figure summarizing simulated spectrometer parameters is produced. This workflow without an actual GUI (graphical user interface) enables more powerful usage, for example automated varying of parameters, searching of optimal conditions, or connection to calculation defining the geometry of the spectrometer. However, an effort has been made to make the usage so simple that only very basic knowledge of Python programming is needed. An example in Appendix B shows a script varying the source to crystal distance and plotting the resolution of such spectrometer as a function of this distance (shown in Fig. 4).

The basic workflow to simulate a spectrometer starts by calling the *mmpxrt.init()* function, set all parameters, then call *mmpxrt.spectrometer()* to run the simulation and then *mmpxrt.spectrometer_evaluate()* to evaluate it and to produce the output. The latter functions works actually with two ray tracing simulations with different source parameters. First one has broadband energy spectrum and asses the properties such as spectral range and dispersion relation. The second simulation with monochromatic beam calculates the point spread function, resolution, efficiency, etc.

Applications which require higher flexibility can skip the *mmpxrt.spectrometer()* routine and go directly to the *mmpxrt.raytrace()* function and simulate basically any geometry in any application. Still, the simulation is designed to study single element (crystal) only. Each ray therefore consists of three points. First, the source point, where the position, initial angle, and energy of a ray are defined. The source position can be either an ideal point or could be random within a sphere to simulate finite source size, or two points to assess the spatial imaging properties and corresponding blurring or deformation of the spectra. Standard setting of beam initial divergence is to assume a spherically divergent source, but for the efficiency of the calculation, the rays are randomly distributed only over the area of the crystal. Other possibilities include a narrow beam with either Gaussian or homogeneous circular profile. Energies of rays can be either monochromatic, dichromatic, broadband, or a custom spectrum can be given.

The second point of each ray corresponds to the reflection point on the crystal. The crystal can be either mosaic or monocrystal. The interaction with monocrystal is quite straightforward; the interaction is more complex if the crystal has a mosaic structure, which is described in the following section. The third point is the intersection of the ray with the detector plane. This plane is theoretically infinite, with arbitrary orientation. For the evaluation algorithm, the real dimensions and pixel size of used detector can be given to produce more easy-to-read results.

3. Mosaicity algorithm

The mosaic crystals are composed of many small crystallites (typically 10s - 100s nm in size) with partially random orientation [2]. Their orientation is described by the mosaic distribution function, i.e. the distribution of their surface deviation from the crystal surface. It was shown that this distribution can be well described by double Lorentzian profile, where one Lorentzian curve with FWHM equal to the mosaicity m models the peak, and a second one, significantly broader,

models a wide background [8]. Still, it is commonly assumed that single Lorentzian is a sufficient model for most cases. The mosaicity (or mosaic spread) m is typically provided by the crystal manufacturer.

The mosaicity is usually estimated as the rocking curve width of the crystal. This rocking curve is measured with a diffractometer, where the intensity of a reflected monoenergetic beam is measured while the angle of incidence on the crystal is varied [8]. This mosaic distribution, whose spread is typically in the order of $0.05° - 2°$, should not be confused with intrinsic crystallite rocking curve width. This value is more difficult to measure experimentally, and typically lies in the order of $0.006°$ [8].

The propagation length of an x-ray within such crystal can be in the order of 10s to 1000s μm. Assuming the crystal is homogeneous with constant attenuation factor, then the intensity I of a beam in depth x in the material is given by the exponential attenuation $I(x) = \exp(-x/\lambda)$, where λ is the penetration depth. In general, λ is a function of x-ray energy and material properties, and is hard to theoretically evaluate for such structured material. The code relies on input of λ from literature or measurement, but it can automatically scale the value to different x-ray energy assuming the energy dependence of λ in mosaic crystal is similar to its dependence in amorphous material (carbon for HOPG and HAPG crystals), and having this dependence tabulated in input. The penetration depth at any energy E is then approximated as:

$$\lambda(E) = \lambda(E_{\mathrm{ref}}) \frac{\lambda_{\mathrm{T}}(E)}{\lambda_{\mathrm{T}}(E_{\mathrm{ref}})}, \qquad (1)$$

where E_{ref} is the x-ray energy at which the reference data $\lambda(E_{\mathrm{ref}})$ was obtained, and $\lambda_{\mathrm{T}}(E)$ is the tabulated penetration depth of the same but non-mosaic material.

The mosaic crystals in the code are defined by their shape (size and curvature), mosaicity m, thickness l, peak reflectivity r (i.e., the reflectivity corresponding to the optimal incidence angle) and penetration depth λ. For each ray, the depth in crystal where they are reflected is obtained from

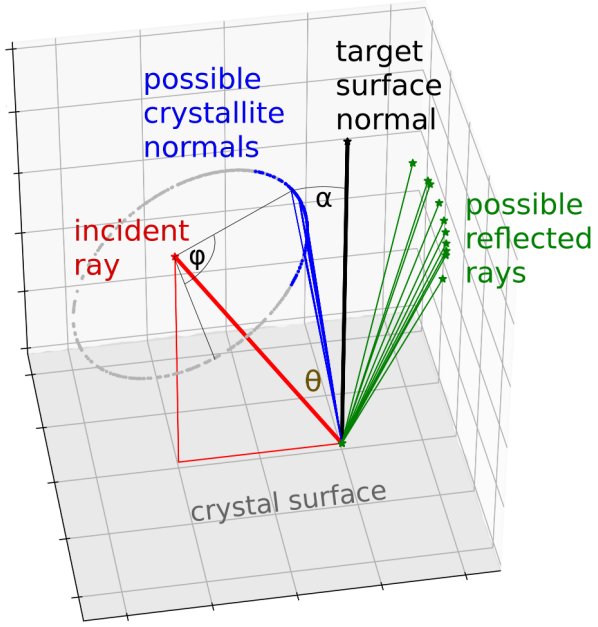

Figure 1: Illustration of the vectors for estimation of the mosaic reflection.

exponential random distribution with coefficient $\frac{\lambda}{2}\sin(\theta_{\mathrm{Bragg}})$, where the sin corrects for the incidence angle of the crystal and the $\frac{1}{2}$ factor is there, because the ray has to penetrate through the crystal to the reflection point and then back to its surface.

Obtaining the angle of reflection from the mosaic crystal is the crucial part of the code, and is illustrated in Fig. 1. The x-ray photon is incident at the angle shown by the vector of the *incident ray* (red). The normal of the crystal surface is marked as black. The angle θ between these two is close to the Bragg angle in order to reflect the ray. At this stage, the code neglects the intrinsic crystallite rocking curve width. With that assumption, the angle between the normal vector of any reflecting crystallite n_c (blue) and the incident ray has to be exactly θ_{Bragg}. This condition defines a circle of all possible solutions (gray), which is in the code parameterized by rotation angle φ. From those solutions, the result has to be selected based on the Lorentzian distribution of the crystallite orientations. Therefore,

the probability $p(\theta, \varphi)$ is calculated by:

$$p(\theta, \varphi) = \frac{1}{\pi m \left(1 + \left(\frac{\alpha(\varphi)}{m}\right)^2\right)}, \tag{2}$$

where $\alpha(\theta, \varphi)$ is the angle between crystal surface and a ray defined by angle φ. The crystallite normal vector defined by a value of φ, and therefore the direction of reflected ray, is randomly selected based on this nonstandard distribution using the rejection sampling method.

The effect of intrinsic crystallite rocking curve width is applied on the reflected beam after this algorithm. It is approximated by tilting the the vector by a random amount in the magnitude of the intrinsic width in a random direction.

Prior to the simulation, the probability is calibrated to correspond to the given reflectivity of the crystal. The probability of reflection of a beam at angle θ is calculated as an integral over all φ:

$$i(\theta) = \int_0^{360^\circ} p(\theta, \varphi) \mathrm{d}\varphi. \tag{3}$$

This probability for the optimal Bragg angle θ_0 should then correspond to the given peak reflectivity r; however, during the simulation, it is assumed that $r = 1$, and the efficiency is corrected for the factor later. For a ray with arbitrary incidence angle θ, the probability of its reflection is then obtained as $r(\theta) = \frac{i(\theta)}{i(\theta_0)}$. This ensures that a ray impinging with the optimal Bragg angle is always reflected, and the probability of reflection is decreasing with increasing deviation.

4. Evaluation

The strength of the code lies in the evaluation tool, which calculate most important performance parameters. Most of those are easy to understand and are therefore only briefly described in the user manual, however the spectral resolution, efficiency and source size broadening deserves a closer attention and are discussed here.

4.1. Spectral resolution

The code calculates three different values as a measure of spectral resolution. All of them are based on the 2D point spread function (PSF) as shown e.g. in Fig. 2. This PSF is an image on detector from a simulation with monoenergetic beam. All methods try to asses a FWHM of the PSF which is in mm, and then can be converted to eV by using the central dispersion obtained from the simulation with broadband spectrum.

The first method plots the vertical profile integrating over horizontal (non-dispersive) direction y, shown as white lineout in Fig. 2. It estimates its FWHM (full width at half maximum) literally as measuring the length of the profile which is above half of its maximum value.

The second method uses the same approach on a region limited in y. This region is marked by red lines in the figure, and the resulting profile is also drawn in red.

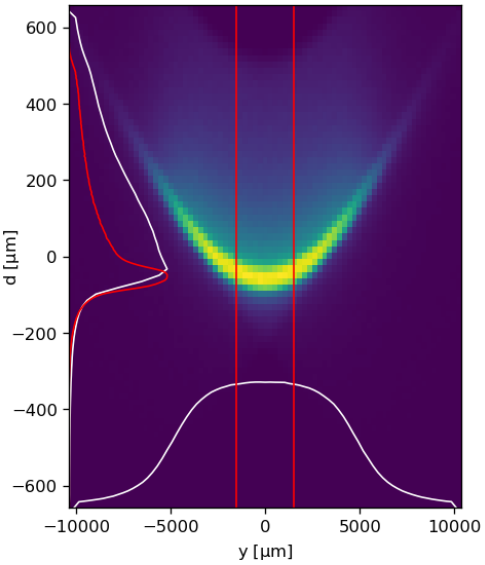

Figure 2: Point spread function, i.e., a signal made by a monochromatic beam on a detector in the spectrometer described in Sec. 5.2 with $d_{\mathrm{SC}} = 730$ mm.

The third method calculates the spread of the points along the vertical (dispersion) direction as a root-mean-square (RMS). This spread is consequently multiplied by 2.3548 in order to correspond to FWHM of Gaussian profile. This means that if the PSF would have a Gaussian profile in d, this would yield the same value as the first

method; the difference between these methods shows how much the PSF differs from Gaussian shape.

4.2. Efficiency

The efficiency of a spectrometer is a crucial value, which often decides which type of instrument should be used. Comparing the efficiency of mosaic and non-mosaic crystals is especially not trivial due to their different physical structure and properties. The efficiency η is calculated as

$$\eta = r\frac{n_{\mathrm{det}}}{n_{\mathrm{gen}}} * \frac{\Omega_{\mathrm{div}}}{4\pi}, \tag{4}$$

where r is the peak reflectivity of the crystal, n_{det} and n_{gen} are the numbers of detected and generated rays, respectively, and the solid angle covered by the source is $\Omega_{\mathrm{div}} = 4\arcsin(\sin(dX/2) * \sin(dY/2)$, dX and dY being the horizontal and vertical divergence of simulated source beam. Since for monocrystals it is more common to work with integrated reflectivity, the peak reflectivity r is obtained as $r = r_i/rcw$, where r_i is the integrated reflectivity and rcw the rocking curve width. This formula obviously assumes square-shaped rocking curve, but is designed such that if only the rocking curve width and integrated reflectivity are known, the efficiency calculation works correctly. For mosaic crystals, the value of peak reflectivity has to be given as an input, as this value is usually experimentally provided, showing a probability of reflection of a ray incident exactly on Bragg angle. As an example, [8] shows a reflectivity map of two HAPG crystals, where the peak reflectivity in the (002) order was varied between $10-50\%$, presents results for higher orders and compares them to previous work [9].

4.3. Source size broadening

Source size broadening is an effect where a finite size of the source decreases the spectral resolution of the measurement. This is caused by the fact, that photons emitted at different source positions are reflected to places on the detector, even if they have the exact same energy. Various spectrometers can have various sensitivity to this effect. The typical way how to asses this is to simulate a larger source size and check the resolution. However, since this would be computationally costly to include into standard spectrometer routine, a more general and stable method is included.

In the simulation with monochromatic source, part of the initial ray positions are shifted by a given spatial offset r_{off}, i.e., instead of having a larger source, two point sources are used. In the evaluation phase, the code measures the spatial offset of the detected signals for these two sources on the detector d_{off}, and calculates a factor $\mathrm{s_{source}}$ as :

$$s_{\mathrm{source}} = \frac{d_{\mathrm{off}}d}{r_{\mathrm{off}}}, \tag{5}$$

where d is the central dispersion evaluated in the broadband run of the simulation. This quantity has a unit of eV/mm, i.e. if multiplied by a source size expected in the experiment, it provides an lower estimate of the spectrometer resolution in eV. In both cases presented in the Appendix of this paper, this value (called *source size broadening*) is around 30 eV/mm.

5. Test cases

This section presents five spectrometer cases and highlight interesting results, showing the modes of operation and benefits of using this code for design and evaluation of experiments. The cases described in this section are also provided as examples within the distribution package.

The first three cases present different features of similar HOPG spectrometers. First case refers to a study of PSF and shows how the penetration depth can be experimentally inferred. Second case studies the mosaic focusing, and the third one presents the spectral envelope of such spectrometer. The fourth case shows how mosaicity can be measured and understood by studies with collimated beam. The fifth case is the only one using a monocrystal, specifically toroidally bent germanium in two different cuts (220 and 400). It shows how sensitive such spectrometer can be to the rotation of the detector.

5.1. Point spread function

The point spread function, i.e., the spectrum observed when the source is monochromatic, is extremely important property of any spectrometer, since it defines its spectral resolution. In spectrometers with monocrystals it is usually narrow and directly related to the rocking curve width of the crystal, however, in mosaic crystals, it can be influenced by several factors and it is not trivial task to tell which is the dominant one.

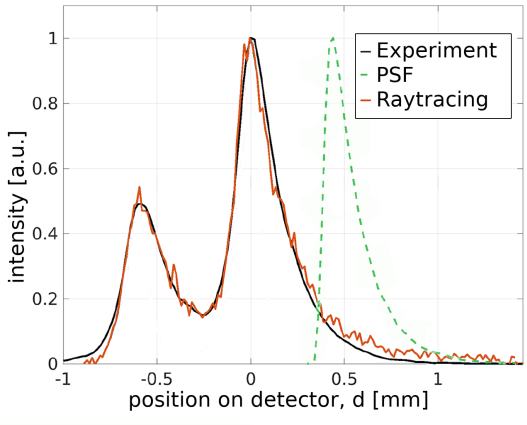

Figure 3: Experimental spectrum fitted by a raytracing simulation by varying the penetration depth.

An experimental study showing the correctness of the PSF modeled by a previous version of this code, as well as estimating the penetration depth of x-rays into the HOPG crystal was published before [4]. Cyllindrically-bent HOPG crystal with mosaicity $m = 0.8°$ and thickness 2 mm was used to measure a Cu K_α radiation at 8047 eV. Due to the thickness of the crystal, the width of the PSF (and therefore the spectral resolution) was dominantly controlled by the penetration of the radiation through the surface of the crystal. This penetration depth was varied in the simulation and the resulting spectra were compared to the experiment. By this way, the value of penetration depth was inferred as $\lambda(E_{\mathrm{ref}}) = 695$ µm at $E_{\mathrm{ref}} = 8047$ eV. Figure 3 shows the agreement of the experimental data with the fitted simulated spectrum and the spectral lineout of the PSF (green, offset for clarity). The value obtained from this measurement is used as a default setting in the code for HOPG crystals.

5.2. Mosaic focusing

The mosaic focusing in x-ray spectrometers defines that in order to have the best spectral resolution, the source - crystal distance has to equal the crystal - detector one, $d_{\mathrm{SC}} = d_{\mathrm{CD}}$ [2]. It is, however, usually not studied how precisely this condition have to be met, or if it can be even violated if e.g. required by experimental constraints.

We present a case motivated by such experimental constraints, where both the minimal source-crystal and maximal crystal-detector distances were given. This spatial limitations have not allowed to use the focused scheme. However, this analysis shows that influence of even 5 cm deviation from ideal setup is perfectly acceptable in this case. This experiment uses a cyllindrically bent 2×4 cm large HOPG crystal with radius of curvature $r = 115$ mm and mosaicity $m = 0.8°$. The distance d_{SC} was varied while crystal-detector distance was fixed at its maximal allowed value of $d_{\mathrm{CD}} = 680$ mm.

Figure 4 shows the variation of the three measures of spectral resolution provided by the code (as discussed in Sec. 4.1) as a function of d_{SC}. The point spread function of the spectrometer, i.e. its response to a monochromatic beam (shown in Fig. 2), has strongly assymetrical shape with relatively narrow peak and long tail in the spectral direction (vertical in figure). The resolution obtained from RMS (blue curve) is therefore significantly different from the one obtained from its FWHM (orange curve). The green curve shows a resolution obtained as FWHM of the response limited to a central 3 mm wide region of the spectrum on detector, as marked by red lines in Fig. 2 and described in Sec.4.1.

It is seen that the d_{SC} distance of 730 mm provides comparable results in terms of spectral resolution as the focused regime ($d_{\mathrm{SC}} = d_{\mathrm{CD}} =$ 680 mm). Note that this shows the resolution decrease due to mosaic defocusing. In a real situation, the resolution can be decreased due to other effects such as source size, detector resolution, crystal imperfection, etc. The script which runs the simulation and produces Fig. 4 is shown in Appendix B as an example.

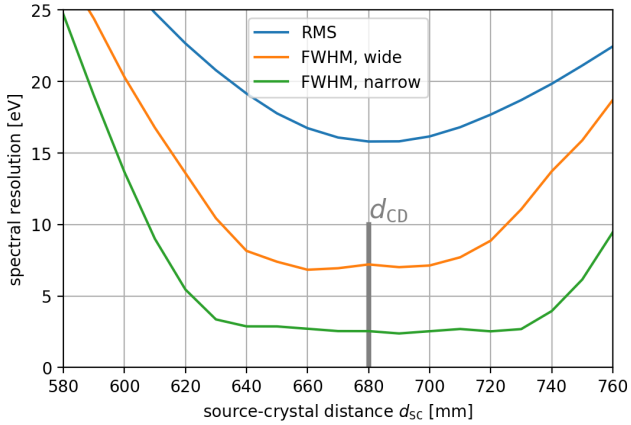

Figure 4: Spectral resolution of spectrometers violating the mosaic focusing condition.

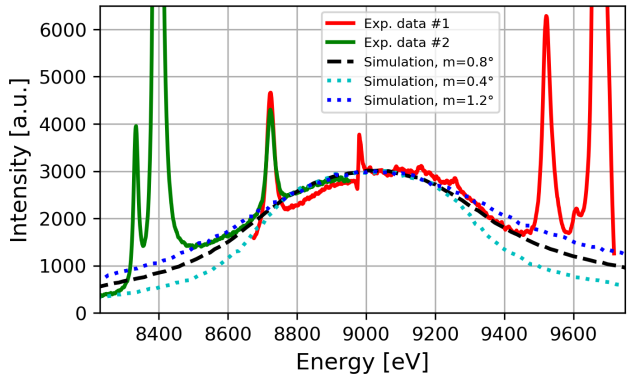

Figure 5: The spectral envelope of a mosaic spectrometer; simulated by the code (dashed) and experimental data (solid).

5.3. Envelope of the spectrum

The x-ray spectrometers are usually set for specific angle of incidence, which corresponds to the so-called central ray, having the central energy. It is common to expect that the instrument performs equally within its whole range. However, for spectrometers where mosaic effects become important (corresponding to $r_m > 1$ as discussed in [4]), the efficiency can significantly drop for rays further from the central one. Therefore it is important to know the spectral envelope, i.e. the response of the instrument to broadband source with a flat spectrum.

Figure 5 shows this envelope, as a lineout of the simulated spectrum, compared with the experimental data. The x-ray source in the experiment was a microfocus x-ray tube with tungsten (W) target, operated at 80 kV and 1.6 mA. The spectrum has been measured by a cylindrically bent HOPG spectrometer with radius of curvature $r = 115$ mm, lattice spacing $2d = 6.708$Å, size 2×4 cm and mosaicity $m = 0.8°$. The distances were set as $d_{SC} = 560$ mm, $d_{CD} = 590$ mm, and the angle of incidence $\theta = 11.9°$ corresponds to the central energy of 8990 eV. As the detector was only 28 mm long, two measurements were performed to extend the observed energy range. The only difference between those sets of data was the translation of the camera by around 10 mm along the energy dispersion direction. The experimental spectrum shows dominant characteristic lines of tungsten over a continuous broadband background emission. It is seen that this background is reasonably well fit by the simulated envelope. This comparison shows the validity of the code in simulating the envelope, which is of significant importance if such spectrometer would be used for analysis of intensities of spectral lines which would be further from each other.

In this setup, the variation of incidence angle over the whole surface of the crystal is relatively small compared to the mosaicity. Therefore, the the envelope (spectral range) is given by the mosaic spread of the crystal. To highlight this dependence, Figure 5 shows also simulations with $m = 0.4°$ and $m = 1.2°$. This also hints that similar measurement can be used to easily estimate or verify the mosaicity.

5.4. Mosaicity studies with collimated beam

This section discusses a method of verification of the mosaicity by using a collimated x-ray beam. A thin collimated (parallel) x-ray beam with energy $E = 8150$ eV is directed towards a flat HAPG crystal with mosaicity $m = 0.08°$ and thickness $D = 30$ µm. The angle of incidence is varied around the optimal Bragg angle (13.11°) to observe the changes in reflected beam. Fig. 6 shows profiles of the reflected beam 25 cm behind the crystal. The horizontal broadening of the spot is caused by the penetration of photons into the crystal, and is given by formula (4) in [1] as

$$2D\cos(\theta) = 58 \text{ µm}. \quad (6)$$

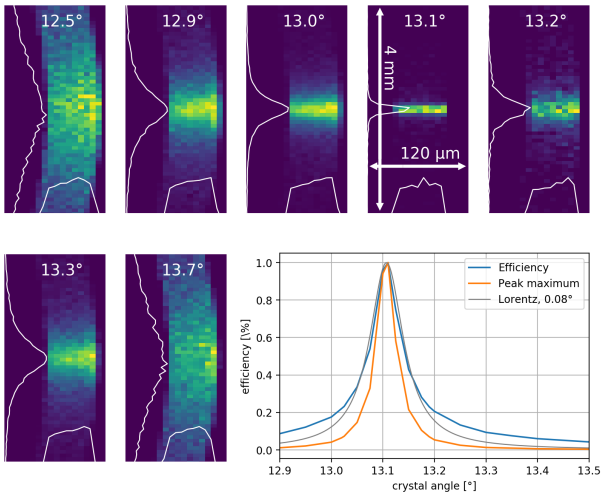

Figure 6: Simulated detected image for various Bragg angles, where 13.1° corresponds to optimal condition.

In the plot for the optimal Bragg angle ($\theta = 13.1°$), the reflected spot has a minimal vertical size, corresponding to $\sin(m) * d_{\mathrm{CD}} = 34$ µm. In cases with higher deviation from the Bragg condition, the vertical size, i.e. the vertical divergence of the reflected beam, rises, because the shape of $p(\theta, \varphi)$ with varying φ is getting broader for sub-optimal θ. This is because in the case with sub-optimal θ, already the 'most optimal' crystallite has already significant deviation from the target surface, so the variation with φ does produce only small relative change.

The plot in Fig. 6 shows the total integrated intensity (i.e. efficiency, blue) and the intensity of the peak of the signal (orange). Both these values might often be confused in experimental estimation of mosaicity. The plot shows that neglecting this effects leads to different shape of the rocking curve. Also, both curves slightly vary from the single Lorentzian curve (gray) due to the complicated nature of mosaic reflection. Experimental study of this phenomena will be a topic of a followup publication.

5.5. Detector rotation

When using focusing toroidal crystals, the orientation of detector is not easy to asses, as different energies are focused in different points, which might actually not lie on a straight line. The simulation can provide a deep insight into which orientation provides best focusing in desired energy range, and an estimation of needed experimental precision.

Here we present two different setups, both using germanium crystals, to observe the radiation around 8.1 keV. The first one uses Ge crystal in 220 cut, with radii of curvatures 1500 mm and 150 mm, source-crystal distance 300 mm and crystal-detector 596 mm, as shown in Fig. 7. The second employs Ge 400 crystal with radii of curvatures 400 mm and 200 mm, source-crystal distance 300 mm and crystal-detector 485 mm, see Fig. 8.

Figures 7 and 8 show the simulated image on the detector for different rotations, where 0° corresponds to detector perpendicular to the incoming beam. The optimal angles are −25° and +70° for Ge 220 and Ge 400, respectively. It is very interesting to see that for the case with Ge 220, a 5° difference in orientation makes hardly any observable difference, but the setup with Ge 400 is significantly more sensitive to this alignment.

6. Conclusions

We have presented a new ray tracing code *mmpxrt* whose primary aim is to help in design and evaluation of x-ray crystal spectrometers, both with monocrystals and mosaic crystals. The code is supplied as a Python3 library, which provides a huge flexibility and possibility to scan any input parameters, but requires a (minimal) programming skills to operate it. It is provided with a set of running examples based on cases presented in this article, and with a user manual. The output of the code summarizes all important parameters needed to evaluate the spectrometer performance in graphical, textual, and data form. This paper have shown several interesting effects simulated in mosaic spectrometers aimed to help experimentalists in understanding and designing similar tools. All presented cases are included within the distribution so that prospective user can build on top of them. Several follow up publications are planned to show the application of this code for experimental design and crosschecking its results with measured data.

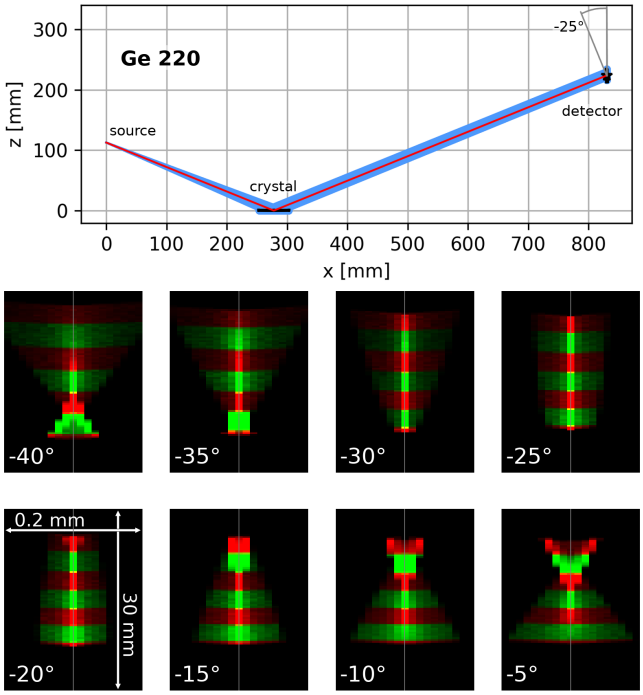

Figure 7: Simulation of the Ge 220 spectrometer. Top pane shows its geometry with marked definition of the angle of the detector. Bottom part shows the detected image for various rotations of the detector, showing that rotation between -20 and -25 provides sufficiently good result. The images are saturated to intensify the wings. Red and green colors are changing each 100 eV to show the range of the instrument.

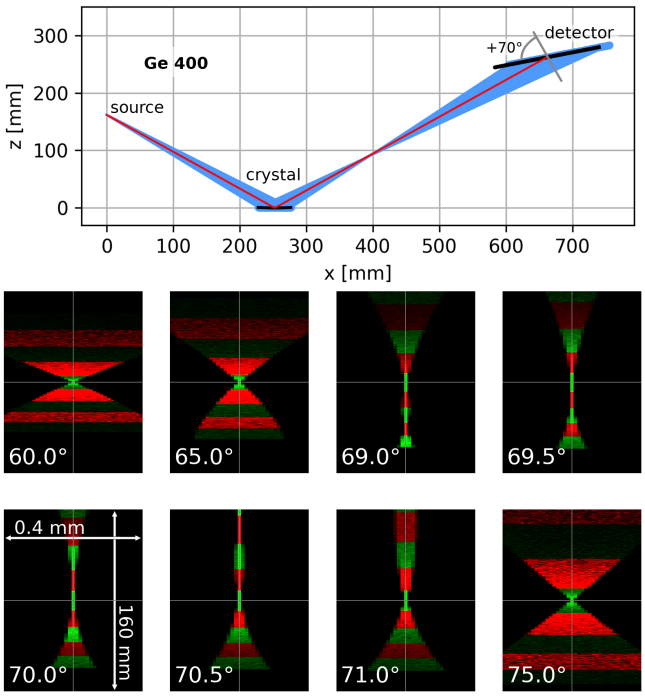

Figure 8: Simulation of the Ge 400 spectrometer. Top pane shows its geometry with marked definition of the angle of the detector. Bottom part shows the detected image for various rotations of the detector, showing that rotation only between 69 and 71 provides a good result. The images are saturated to intensify the wings. Red and green colors are changing each 50 eV to show the range of the instrument.

7. Acknowledgments

This research was supported by the Helmholtz Association under the grant no. VH-NG-1338.

Appendix A. Standard output

The code automatically present the most useful results in an overview figure. Examples of such output is in Figures A.9 and A.10 for for simulations with mosaic crystal and monocrystal, respectively. The figures might not be self-explanatory in order to keep things concise, the meaning of each subfigure is written in here:

Geometry (side): The 2D-side view of the spectrometer. The crystal lies in the X-Y plane at $z = 0$, i.e. in the bottom of the figure. The source is on the left, having $x = 0$, the detector is on the right-hand side. The actual crystal and detectors are drawn in black. The central ray is drawn with orange, and all other rays are in light blue.

Dispersion: The simulated dispersion of the spectrometer. The horizontal axis is the *detector* axis d[mm], i.e. the dispersion axis in in the detector plane, where d=0 is where the central ray is impinging the detector. The detector surface is therefore parameterized by two axis: d and y. Each blue point represents one ray, showing its energy [eV] and its position on the detector. All those points are fitted by quadratic dispersion (orange), and the tangent at $d = 0$ is shown in black. The vertical gray lines show the physical extent of the detector, the horizontal ones project this extent to the energy scale, showing the real spectral range.

AOI on the crystal: This figure represents the top view on the crystal. The thick black lines shows outline and diagonals of the crystal. Only the central part of the crystal might be seen in

some cases, then the diagonals help to see how small part is shown. The intersection of the rays from the *monochromatic* simulation with the crystal are marked as circles whose color correspond to the deviation of the angle of incidence of each ray from the Bragg condition. This means that the region filled with circles is the active region of the crystal for single energy, and the range of shown angles corresponds to either the rocking curve width or to the mosaicity.

Detector image: The image of the *broadband* simulation as would be seen on detector. It is a 2D histogram, where intensity of each pixel corresponds to the density of rays hitting the region. Furthermore, the rays are distinguished into red and green colors according to their energy in order to give the impression of the range and resolution of the instrument. The code automatically selects a suitable stripe width (100 eV in Fig. A.9), and the photons are 'changing' the color each 50 eV. The thick white line is the vertical lineout of this image, i.e. the spectral envelope. The thin yellow line is the lineout of 'green' rays, so that the sharpness of its edges shows the spectral resolution.

Point spread function: The detected image of the *monochromatic* simulation; this is more discussed in Sec. 4.1, as this data are crucial to infer the spectral resolution.

3D view shows the overview of the spectrometer geometry, similar as the first subfigure.

Appendix B. Example of input file

Below is an example of an input file in a structure of Python script, which generates Fig. 4. The first part initializes variables to store the results. The *for* cycle goes through different source-crystal distances d_{SC}, for each it initializes the ray tracing, set up simulation parameters and geometry, and runs the simulation via *mmpxrt.spectrometer()*. The rest of the file makes a plot of the dependence of the resolution on the distance.

```
#!/usr/bin/env python3
import mmpxrt
import numpy as np
import matplotlib.pyplot as plt

dscs=np.arange(580,770,10) #Dsc to be simulated
res1=np.zeros(dscs.size) #arrays for simulated resolutions
res2=np.zeros(dscs.size)
res3=np.zeros(dscs.size)
for di,dsc in enumerate(dscs):
    p=mmpxrt.init()
    p['source']['EcentralRay']=9040
    p['source']['EmaxBandwidth']=1000
    p['source']['divergenceFWHM']=-1 #automatic

    p['crystal']['d2']=6.708
    p['crystal']['mosaicity']=0.8

    p['crystal']['width']=20
    p['crystal']['length']=40
    p['crystal']['radius_l']=1e9
    p['crystal']['radius_w']=115
    p['crystal']['crystalPeakReflectivity']=0.45
    p['crystal']['maxThickness']=30e-3
    p['crystal']['thickness']=-1 #use exponential dist.

    p['geometry']['detRot']=0
    p['geometry']['evaluation_width']=3
    p['geometry']['CrystalSource']=dsc
    p['geometry']['CrystalDetector']=680
    p['geometry']['evaluation_width']=3
    p['geometry']['detectorLength']=40
    p['geometry']['detectorPxSize'] = 5e-3

    p['simulation']['numraysE']=-1
    p['simulation']['numraysB']=1e6 #rays for broadband sim.
    p['simulation']['numraysM']=1e7 #rays for monochrom.sim.
    p['simulation']['name']='Dsc-{:2d}'.format(dsc);
    p['simulation']['comment']='MMpXRT simu., Michal Smid'
    p['simulation']['num_processes']=15

    rrrs = mmpxrt.spectrometer(p) #the simualtion itself

    disp=p['evalu']['dispersionLinearCentral']
    res1[di]=p['evalu']['verticalSpreadRMS']*disp
    res2[di]=p['evalu']['verticalSpreadFWHM']*disp
    res3[di]=p['evalu']['verticalSpreadFWHMNarrow']*disp

# %% Drawing the output figure
plt.plot([680,680],[0,10],linewidth=3,color=[0.5,0.5,0.5])
plt.plot(dscs,res1,label='RMS')
plt.plot(dscs,res2,label='FWHM, wide')
plt.plot(dscs,res3,'-',label='FWHM, narrow')
plt.grid()
plt.legend()
plt.xlabel("source-crystal distance $d_\mathtt{{SC}}$ [mm]")
plt.ylabel("spectral resolution [eV]")
plt.ylim(0,25)
plt.xlim(580,760)
plt.text(680,10.5,'$d_\mathtt{{CD}}$')
plt.xticks(np.arange(580,780,20))
plt.savefig('Fig7.png' , bbox_inches ='tight',dpi=200)
```


[1] G. Ice, C. Sparks, Mosaic crystal x-ray spectrometer to resolve inelastic background from anomalous scattering experiments, Nuclear Instruments and Methods in Physics Research Section A: Accelerators, Spectrometers, Detectors and Associated Equipment 291 (12) (1990) 110 – 116. doi:10.1016/0168-9002(90)90043-6.

[2] H. Legall, H. Stiel, M. Schnürer, M. Pagels, B. Kangießer, M. Müller, B. Beckhoff, I. Grigorieva, A. Antonov, V. Arkadiev, A. Bjeoumikhov, An efficient X-ray spectrometer based on thin mosaic crystal

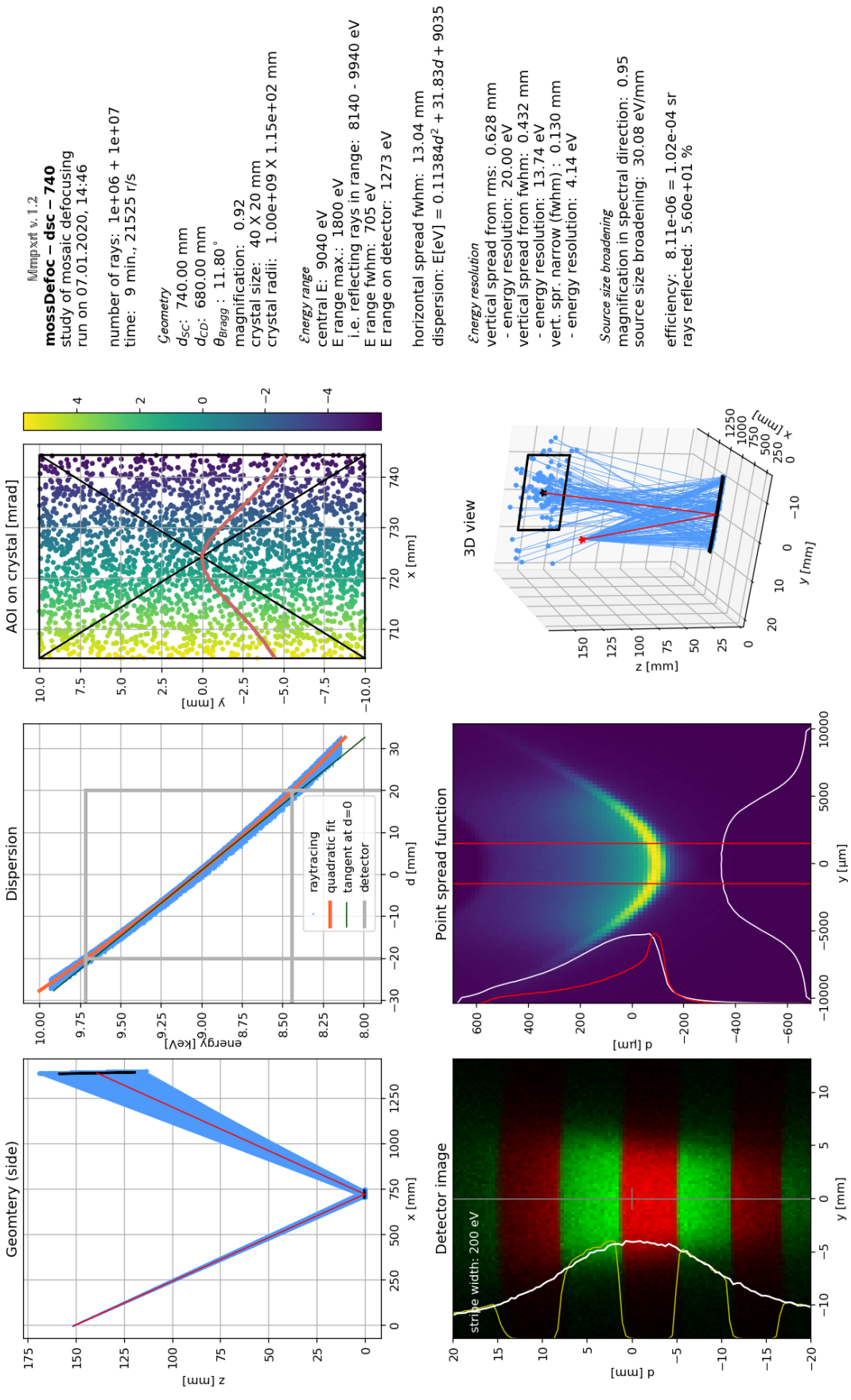

Figure A.9: Graphical output of the simulation with mosaic crystal described in Sec. 5.2.

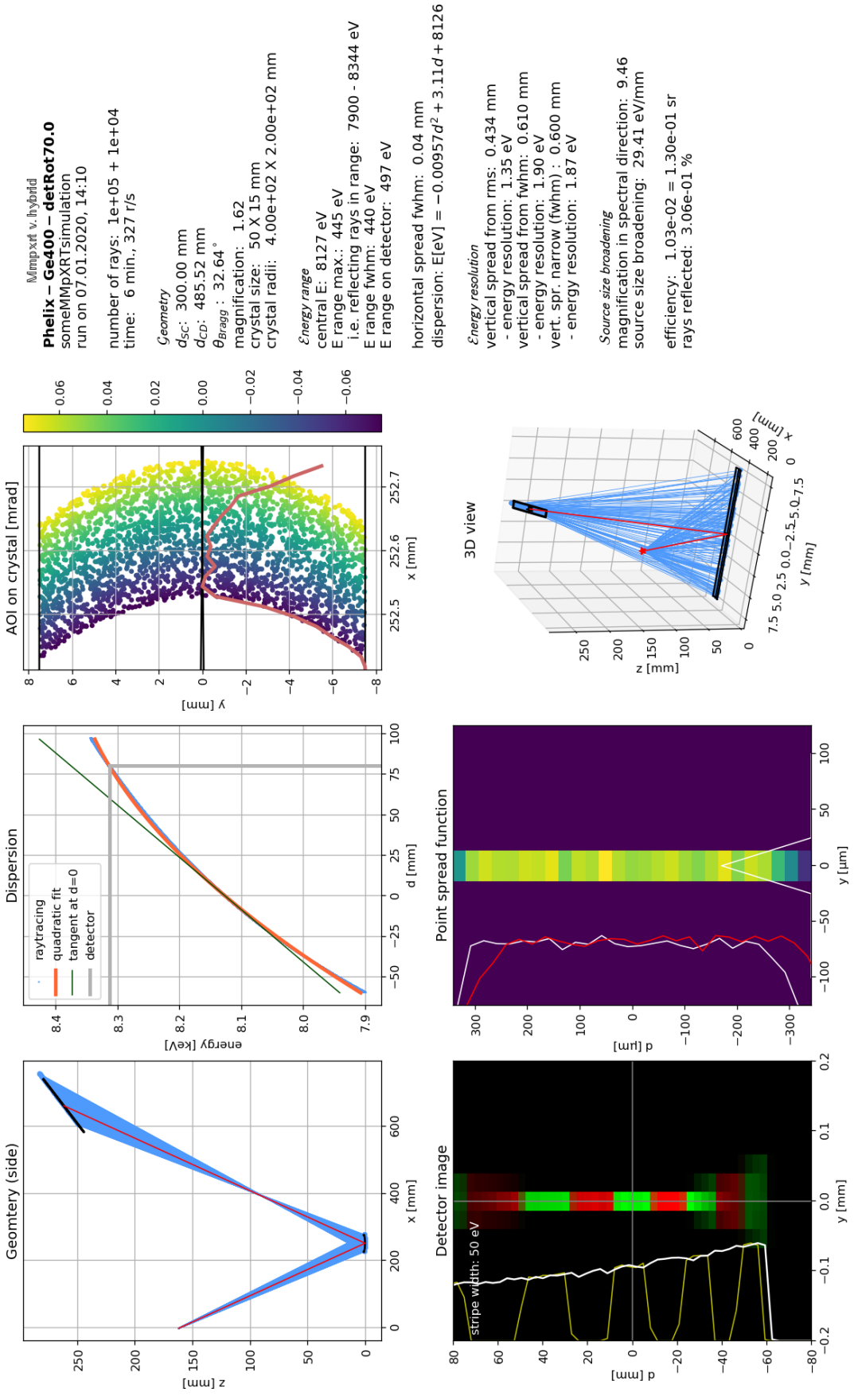

Figure A.10: Graphical output of the simulation with Ge(400) crystal described in Sec. 5.5.

films and its application in various fields of X-ray spectroscopy, Journal of Applied Crystallography 42 (4) (2009) 572–579. doi:10.1107/S0021889809006803.

[3] E. J. Gamboa, D. S. Montgomery, I. M. Hall, R. P. Drake, Imaging x-ray crystal spectrometer for laser-produced plasmas, Journal of Instrumentation 6 (04) (2011) P04004–P04004.

[4] M. Šmíd, I. Gallardo Gonzalez, H. Ekerfelt, J. Bjrklund Svensson, M. Hansson, J. C. Wood, A. Persson, S. P. D. Mangles, O. Lundh, K. Falk, Highly efficient angularly resolving x-ray spectrometer optimized for absorption measurements with collimated sources, Review of Scientific Instruments 88 (6) (2017) 063102. doi:10.1063/1.4986464.

[5] M. Sanchez del Río, S. Bernstorff, A. Savoia, F. Cerrina, A conceptual model for ray tracing calculations with mosaic crystals, Review of Scientific Instruments 63 (1) (1992) 932–935. doi:10.1063/1.1143784.

[6] B. Lai, F. Cerrina, Shadow: A synchrotron radiation ray tracing program, Nuclear Instruments and Methods in Physics Research Section A: Accelerators, Spectrometers, Detectors and Associated Equipment 246 (1) (1986) 337 – 341. doi:https://doi.org/10.1016/0168-9002(86)90101-4.

[7] U. Zastrau, C. R. D. Brown, T. Dppner, S. H. Glenzer, G. Gregori, H. J. Lee, H. Marschner, S. Toleikis, O. Wehrhan, E. Frster, Focal aberrations of large-aperture HOPG von-hàmos x-ray spectrometers, Journal of Instrumentation 7 (09) (2012) P09015–P09015. doi:10.1088/1748-0221/7/09/p09015.

[8] M. Gerlach, L. Anklamm, A. Antonov, I. Grigorieva, I. Holfelder, B. Kanngießer, H. Legall, W. Malzer, C. Schlesiger, B. Beckhoff, Characterization of HAPG mosaic crystals using synchrotron radiation, Journal of Applied Crystallography 48 (5) (2015) 1381–1390. doi:10.1107/S160057671501287X.

[9] U. Zastrau, A. Woldegeorgis, E. Frster, R. Loetzsch, H. Marschner, I. Uschmann, Characterization of strongly-bent hapg crystals for von-hmos x-ray spectrographs, Journal of Instrumentation 8 (10) (2013) P10006. doi:10.1088/1748-0221/8/10/P10006.